Journal of Al-Azhar University Engineering Sector

Vol. 20, No. 74, January 2025, 450-465

NUMERICAL ANALYSIS OF ENHANCING LATENT HEAT STORAGE USING FINS AND CONDUCTIVE BARRIERS

Ahmed A. Al Shafai[1*], E.A. Abdel Hadi[1], S.H. Taher[1], Mohamed R. Salem [1,2], Ashraf E. Elmohlawy[1]

[1] Mechanical Engineering Department, Faculty of Engineering at Shoubra, Benha University, 108 Shoubra St., 11629, Cairo, Egypt

[2] Department of Mechanical Engineering, Faculty of Engineering, Al Baha University, 65527, Al Baha, Saudi Arabia

***Correspondence:** eng.ahmedalshafai@gmail.com

Citation:

A.A. Al Shafai, E.A. Abdel Hadi, S.H. Taher, M.R. Salem, A.E. Elmohlawy, "Numerical Analysis of Enhancing Latent Heat Storage Using Fins and Conductive Barriers", Journal of Al-Azhar University Engineering Sector, vol. 20, pp. 450-465, 2025.

Received: 03 November 2024

Revised: 29 December 2024

Accepted: 30 January 2025

DoI: 10.21608/auej.2025.332683.1727

ABSTRACT

This study conducts a numerical investigation into the performance of a Latent Heat Thermal Energy Storage System (LHTESS), analyzing various configurations and operational parameters to identify optimal strategies for enhancing thermal performance. The study specifically focuses on the impact of different configurations of separation barriers attached to semicircular tubes, both finned and non-finned, in conjunction with varying Heat Transfer Fluid (HTF) temperatures. The results reveal that higher HTF temperatures significantly improve thermal effectiveness, with 85°C achieving a 90% melting fraction in just 79 minutes, compared to only 28% at 65°C. Additionally, incorporating conducting fins reduces charging times by 40%, improving heat transfer and temperature distribution within the Phase Change Material (PCM). Full conducting barriers also enhance both melting fractions and overall performance, particularly in designs with complete barriers. Furthermore, the combination of fins and barriers results in substantial improvements, with Case 2C showing the highest effectiveness at 45.5%. These findings offer valuable insights into the future design and application of LHTESS, advancing the development of more efficient energy management solutions.

KEYWORDS: Thermal Storage Unit, Semicircular tube, PCM, Melting Fraction, Effectiveness.

التحليل العددي لتحسين تخزين الحرارة الكامنة باستخدام الزعانف والحواجز الناقلة

احمد عاطف الشافعي[1*]، عيد عبدالحافظ عبدالهادي[1]، شريف هادي طاهر[1]، محمد رضا سالم[1،2]، أشرف السيد المحلاوي [1]

[1] قسم الهندسة الميكانيكية، كلية الهندسة بشبرا، جامعة بنها، القاهرة، مصر

[2] قسم الهندسة الميكانيكية، كلية الهندسة، جامعة الباحة، الباحة، المملكة العربية السعودية

***البريد الإلكتروني للباحث الرئيسي:** eng.ahmedalshafai@gmail.com

الملخص

يتم في هذا البحث دراسة عددية لأداء نظام تخزين الطاقة الحرارية باستخدام الحرارة الكامنة، حيث يتم تحليل التكوينات والمعايير التشغيلية المختلفة لتحديد الاستراتيجيات المثلى لتحسين الأداء الحراري. تركز الدراسة بشكل خاص على تأثير التكوينات المختلفة للحواجز الفاصلة للحواجز الفاصلة المرفقة بالأنابيب نصف الدائرية، سواء كانت مزودة بالزعنفة أو غير مزودة بها، بالتزامن مع تغيير درجات حرارة سائل نقل الحرارة. تكشف النتائج أن درجات الحرارة الأعلى للسائل الناقل للحرارة تحسن بشكل كبير من الفاعلية الحرارية، حيث تحقق درجة حرارة ٨٥ درجة مئوية نسبة انصهار تصل إلى ٩٠٪ في ٧٩ دقيقة فقط، مقارنة بـ ٢٨٪ عند درجة حرارة ٦٥ درجة مئوية. بالإضافة إلى ذلك، يقلل دمج الزعانف الموصلّة من أوقات الشحن بنسبة ٤٠٪، مما يحسن انتقال الحرارة وتوزيع الحرارة داخل مادة تغيير الطور. كما أن استخدام الحواجز الموصلّة بالكامل يعزز من نسب الانصهار والأداء العام، خصوصًا في التصاميم التي تحتوي على حواجز كاملة. علاوة على ذلك، يؤدي الجمع بين الزعانف والحواجز إلى تحسينات كبيرة، حيث يظهر الحالة 2C أعلى فاعلية بنسبة ٤٥,٥٪. تقدم هذه النتائج رؤى هامة لتصميم وتطبيق أنظمة تخزين الطاقة الحرارية باستخدام الحرارة الكامنة في المستقبل، مما يسهم في تطوير حلول أكثر كفاءة لإدارة الطاقة.

الكلمات المفتاحية: وحدة التخزين الحراري، أنابيب شبه الدائرية ، مواد تغيير الحالة، نسبة الانصهار، التأثير الحرارى.

1. INTRODUCTION

The rapid growth in global population and industrialization has significantly increased energy demand, raising concerns about energy security, global warming from fossil fuel consumption, greenhouse gas emissions, and resource depletion. Renewable energy, particularly solar energy, offers a promising alternative, but its variability poses reliability challenges. To address this, LHTESSs using PCMs have been integrated into solar technologies like PVT panels, solar collectors, and domestic hot water systems [1-6]. Enhancing LHTESS performance is crucial, with strategies such as nano-additives [7], multiple PCMs [8], porous media [9], geometric modifications [9-12], and advanced fins [13-14]. While longitudinal fins improve heat transfer, issues like uneven heat distribution and un-melted PCM regions remain, necessitating further optimization [15-22].

Continuous and fractioned fin distributions with nano additives investigated, concluding that fins were more effective than nano additives in improving LHTESS performance [23]. Y-fin designs exanimated [24, 25], spiral fins reducing melting and solidification times by 57.6% and 74.13%, respectively [26]. Also, spiral fins in vertical LHTESS reduced charging time by 41.48% and discharging time by 22.16% [27]. PCM melting optimization by using simultaneous convection and conduction zones for improved performance [17]. Vertically arranged multi-tube fin configurations achieving the best melting performance [18]. Smaller and closely spaced copper fins leads to optimal heat transfer [19], circular longitudinal fins outperformed traditional designs [20]. Using non-uniform fins reduced charging and discharging times by 24.5% and 16.5%, respectively, [21]. Honeycomb cells with encapsulated PCM significantly improved heat transfer, with cell size and thickness being critical factors [22]. Highlighted the effectiveness of optimized tube and fin configurations in PVT systems [28], while triangular fins achieved a 30% enhancement in solidification rates [29]. Trapezoidal fins studied and reduced solidification time by 45% [30], fractal tree-shaped fins improved both charging and discharging processes with better uniformity [31]. Melting challenges raised with branched fins and reducing longer charging periods [32], finned tubes with nanoparticles reduced charging time by 12.5%–40% [33]. Triangular fins were more efficient than rectangular ones [34]. higher HTF temperatures and flow rates significantly enhanced heat transfer in multitube LHTESS units [35]. Spiral fins at angles of 0°, 45°, and 90° reduced melting time by 51%, 40%, and 34%, respectively [36]. Straight-angled fins is the optimal configuration for melting performance [37], and partial fins reduced melting time by 68% [38]. Advanced PCM shapes introduced and reduced charge/discharge times by up to 50% [39], various configurations of frustum tubes exanimated in storage system [40]. Arc-shaped fins adopted [41], Y-shaped integrated in storage system [42]. Heat transfer improved by 20.77% using converging-diverging tube shapes [43]. energy enhanced storage by incorporating micro-encapsulated PCM, achieving a 16% energy increase [44]. Heat exchanger varies designs exanimated to reduce and improve charging time [45]; Thermal effectiveness improved by using anisotropic metal foams leads to reduce liquefaction times by up to 13.12% [46].

The literature underscores the importance of efficient heat storage mechanisms in Latent Heat Thermal Energy Storage Systems (LHTESS) to ensure continuous operation. While many studies have explored the impact of fins on enhancing LHTESS performance, they often overlook the broader aspects of thermal efficiency and fail to consider the role of partitioning the PCM into smaller volumes, which can significantly enhance system performance and optimize the overall dimensions of the thermal storage unit. This study looks to address these gaps by investigating the combined effects of conducting fins and barriers, with various configurations, on semicircular tubes within cylindrical geometries. Specifically, the research focuses on how different HTF inlet temperatures influence thermal performance, melt fraction, temperature distribution, and total melting time. By examining the synergistic effects of conducting fins and high thermal conductivity barriers in finned semicircular tubes, this study aims to improve heat transfer rates, reduce PCM volume, and introduce barrier separation to further enhance the efficiency of thermal energy storage systems. These improvements contribute to optimizing both renewable energy applications and low-temperature heat recovery, ultimately promoting sustainability and advancing the development of more efficient energy storage solutions.

2. PROBLEM DEFINITION AND SOLUTION METHODS

Designing an efficient PCM storage system involves addressing several intricate phenomena that traditional simulation methods often struggle to fully capture. This study employs a finite element model developed using ANSYS Fluent to optimize the thermal energy storage system. Fig. 1 shows the detailed geometry of the shell and tube heat exchanger used here. A total of 14 different configurations are evaluated, including a baseline design without fins and variations in the number and orientation of the fins. The system features a vertical shell-and-tube heat exchanger where hot water, functioning as the HTF, flows upward through a semicircular tube with an equivalent diameter of 8.3 mm. The 14 configurations are analyzed using copper tubes with external and internal diameters of 9.52 mm and 8.3 mm, respectively. Rectangular copper fins, 1.22 mm thick and extending 15 mm from the tube's outer surface, are used, with the total fin length matching the shell length of 300 mm. The tubes are housed within a carbon steel shell with a wall thickness of 6.2 mm, an internal diameter of 120 mm, and a length of 300 mm. The setup also includes two headers to distribute and collect the HTF, copper barriers, and a 220 mm carbon steel slip-on flange to complete the system.

The study is organized into two groups, as depicted in Fig. 1. The first group **(Case-1)** investigates the effect of integrating copper barriers inside the shell to partition the PCM into smaller volumes, covering 7 cases (1A to 1G). The second group **(Case-2)** focuses on the addition of longitudinal rectangular fins to the outer surface of the semicircular tubes, alongside the copper barriers, covering 7 more cases (2A to 2G). The detailed characteristics of the fourteen configurations analyzed are provided in **Table 1**.

Table 1: Characteristic of different configurations for each case.

Arrang. No.	$D_{sh,in}$ (mm)	L (mm)	$D_{t,o}$ (mm)	$D_{t,in}$ (mm)	Barriers	Fins	N	θ	n	ϕ	λ
1A	120	300	9.52	8.3	W/O	Not Applied	Double Layer Tubes	45°	9	0.024	1st layer: λ = 1/3; 2nd layer: λ = 2/3
1B					W/O						
1C					FPB						
1D					HPB						
1E					FPIB						
1F					HPIB						
1G					FCIB						
2A					HCIB	Applied					
2B					FPB						
2C					HPB						
2D					FPIB						
2E					HPIB						
2F					FCIB						
2G					HCIB						

W/O: Without,
HPB: Half Parallel Barriers,
FPIB: Full Parallel Inclined Barriers,
HPIB: Half Parallel Inclined Barriers,
FCIB: Full Contradiction Inclined Barriers,
HCIB: Half Contradiction Inclined Barriers
FPB: Full Parallel Barriers,
θ : Angle of semicircular tubes from X axis (degrees)

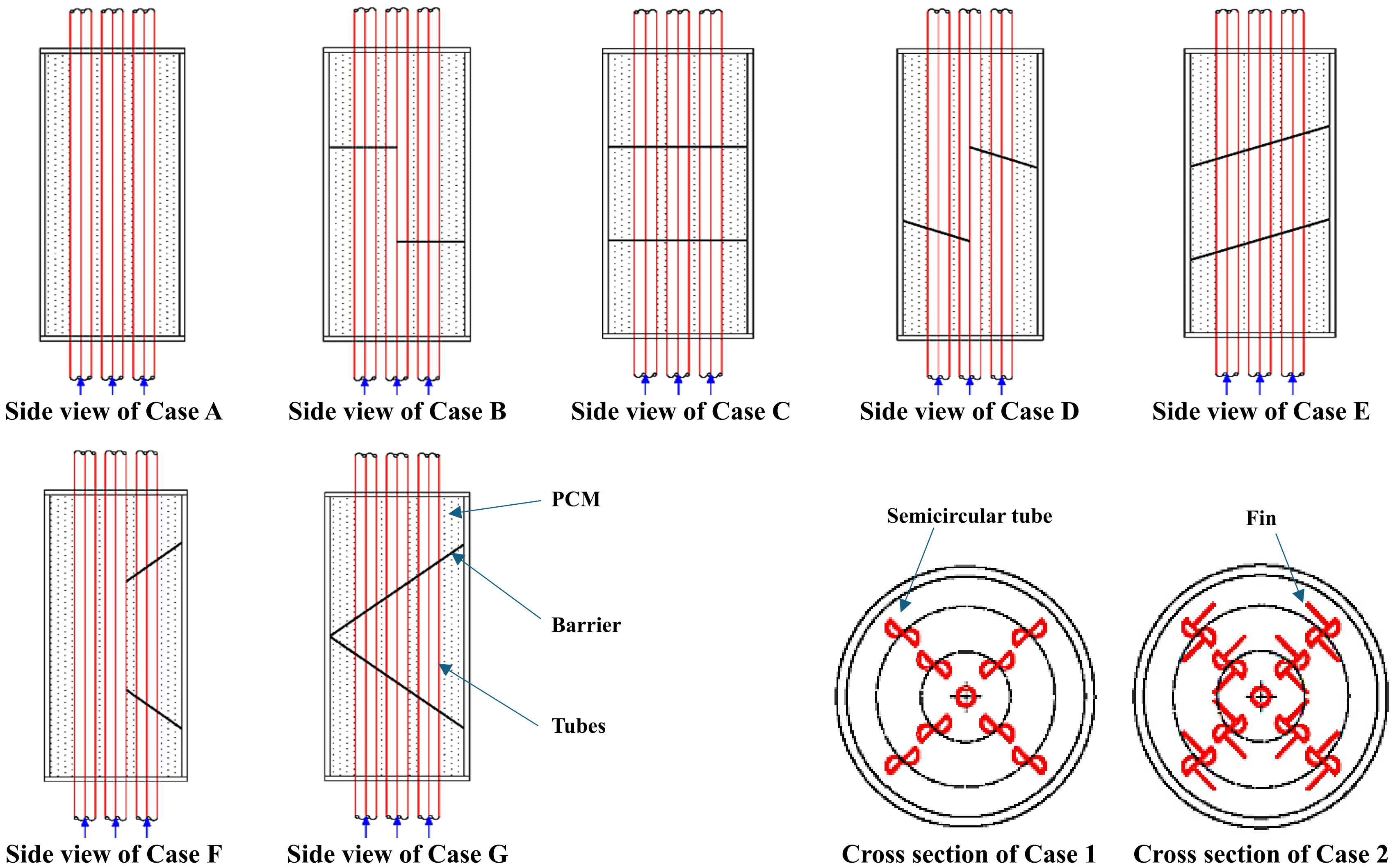

Fig. 1: Schematic diagrams for the various cases of shell and tube storage unit adopted in this study (Cases 1A – 1G) without fins and (Cases 2A – 2G) with attached fins.

The area ratio (ϕ) and radius ratio (λ) are defined as shown in Eqs. (1) and (2), respectively. The D_{layer} expresses the diameter at which the tubes are located.

$$\phi = \frac{n\, A_{t,o}}{A_{sh,in}} = \frac{n\, D_{t,o}^2}{D_{sh,in}^2} \quad \textbf{(1)}$$

$$\lambda = \frac{D_{Layer}}{D_{sh,in}} \quad \textbf{(2)}$$

3. GOVERNING EQUATIONS FOR THE FINITE ELEMENT MODEL

To analyze the heat transfer process during the melting of PCM within a LHTESS, a 3-D transient numerical model is utilized in Fluent. The thermophysical properties of paraffin wax represent PCM used in the present investigation, are given in **Table 2** [47], and are consistent with those used in the experimental setup. The initial temperature of the solid paraffin is set at 25°C. For $\tau > 0$, hot water is circulated through the LHTESS.

Table 2: Thermophysical properties of paraffin wax and HTF (water) used in the present study.

Property	Melting temperature (°C)	Latent heat (J/kg)	Specific heat (J/kg.°C)	Density (kg/m^3)	Thermal conductivity (W/m.°C)	Viscosity (Pa.s)	Thermal expansion coefficient (1/K)
Paraffin wax [47]	54	114540	1465 (liquid)	820 (liquid at 54°C)	0.14 (solid at 30°C)	0.033 (at 65°C)	6×10^{-4}
Water	---	---	4190	996	0.66	0.001	2.1×10^{-4}

The model for the LHTESS incorporates several governing equations and assumptions to accurately simulate the heat transfer process. Water, used as HTF for both charging and discharging process, is treated as incompressible, Newtonian, and unsteady. The flow within the inner semicircular tubes is assumed to be turbulent, determined by the Reynolds number. The outer shell is insulated to prevent heat loss to the surrounding environment. To simulate the phase change of the PCM, the enthalpy-porosity method is employed. A 3-D transient study is conducted using the Boussinesq approximation, which treats the fluid as incompressible, except for buoyancy effects in the momentum equations. The standard k-ε turbulence model is applied to capture the turbulent water flow. Three computational domains are considered in the simulation; Domain 1: Water (HTF) flow, Domain 2: HTF pipe and fins, and Domain 3: PCM. The thermal resistance of the tube and fin materials is incorporated to improve the accuracy of the simulation. Besides, the following assumptions are made for numerical modeling:

1 Only half of the LHTESS is simulated to reduce the computational time.

2 To account for density variation, a source term is added to the momentum equation based on temperature differences, following the Boussinesq approximation.

3 The density variation is calculated using the published method [47], as introduced in Eq. (3):

$$\Delta\rho = \rho\gamma(T - T_L) \quad \textbf{(3)}$$

According to these assumptions, the governing equations for analyzing this problem can be summarized as follows:

Conservation *of mass:*

$$\nabla . \vec{v} = 0 \quad \textbf{(4)}$$

Conservation of momentum:

$$\rho\frac{\partial\vec{v}}{\partial\tau} + \rho(\vec{v}.\nabla)\vec{v} = -\nabla P + \mu\,\nabla^2\vec{v} + \rho\gamma g(T - T_L) + S \quad \textbf{(5)}$$

Conservation of energy:

$$\frac{\partial}{\partial t}(\rho H) + \nabla.(\rho\,\vec{v}\,H) = \nabla.(k\nabla T) \tag{6}$$

The total enthalpy (H) in Eq. (7) is determined by combining the sensible (L_{se}) and latent (L_{th}) heat of the PCM. To calculate these components, Eqs. (8) and (9) are applied:

$$H = L_{se} + L_{th} \tag{7}$$

$$L_{se} = L_{ref} + \int_{T_{ref}}^{T} C\,dT \tag{8}$$

$$L_{th} = \alpha L_m \tag{9}$$

In this study, the enthalpy-porosity method is employed to simulate the phase change during the melting process. This method models the entire computational domain as a porous medium, where the porosity in each computational cell is directly related to the liquid volume fraction present in that cell. The impact of the porous structure on fluid movement is captured by adding a source term to the momentum equation, denoted as (S), which appears on the right-hand side of Eq. (10). This source term is calculated using the following expression:

$$S = A_{mushy}\,\rho\frac{(1-\alpha)^2}{\gamma^3 + Z} \tag{10}$$

In this context, A_{mushy} is a constant that governs the damping effect within the mushy zone, where partial melting or solidification occurs. The parameter α, representing the liquid fraction, determines how much the velocity is reduced as the region solidifies; specifically, as α approaches zero, the velocity in the solidified region is effectively reduced to zero. Additionally, γ is introduced as a small number to prevent division by zero in the equation, while C serves as a regularization parameter to ensure numerical stability. This method effectively slows the fluid flow in regions that remain partially or fully solid, ensuring that the velocity diminishes appropriately during the phase transition from solid to liquid. Earlier studies [48, 49], have demonstrated that the influence of the mushy zone constant A_{mushy} becomes negligible for values exceeding 10^5. Based on these findings, a default value of 10^5 is selected for this study.

The enthalpy-porosity method [47], offers a key advantage in modeling phase change processes: it eliminates the need to explicitly track the solid-liquid interface. Instead, it leverages the relationship between latent heat and temperature, assuming that the latent heat is absorbed linearly across the temperature range between the surface temperature T_s and the liquidus temperature T_L within the mushy zone. The liquid fraction α is then calculated using Eq. (11). This approach simplifies the computational modeling of phase changes, allowing for efficient and accurate simulations of melting and solidification processes. In addition, to accurately simulate the fluid flow and heat transfer characteristics along the wall for turbulent flow inside the water tube, the k-ε model with enhanced wall treatment is employed as the near-wall treatment.

$$\begin{cases} \alpha = 0 & \text{for} \quad T < T_s \\ \alpha = \dfrac{T - T_s}{T_l - T_s} & \text{for} \quad T_s < T < T_L \\ \alpha = 1 & \text{for} \quad T > T_s \end{cases} \tag{11}$$

During the charging process, the melted mass of the PCM over time is tracked by continuously summing the mass of elements whose average temperature exceeds the material's melting point at each time step. This cumulative approach allows for an accurate estimation of the phase change progression within the system. The Melted Mass Fraction (MMF) is then determined as the ratio of the melted mass (m_m) to the total mass of the PCM, providing a clear indication of the extent of melting. Mathematically, this is expressed by summing the melted mass of individual elements, denoted as $m_{m,i}$, which is based on both the mass and volume of each melted element $V_{m,i}$, as represented in Eq. (12). The relationship captures the dynamic evolution of the melting process, helping quantify the energy absorption and phase transition efficiency. This calculation of MMF is critical for assessing the thermal performance of PCM systems, as it provides insight into how effectively thermal energy is being stored in the latent heat phase.

$$\mathrm{m_m} = \sum \mathrm{m_{m,i}} = \rho_s * \sum \mathrm{V_{m,i}} \quad \textbf{(12)}$$

$$\mathrm{MMF} = \frac{\mathrm{m_m}}{\mathrm{m_t}} \quad \textbf{(13)}$$

4. NUMERICAL APPROACH

In this study, a mass flow rate of 15 L/min is applied at the water tube's inlet with outlet atmospheric pressure. The PCM starts at room temperature (25°C), with the inlet water temperature set to 65°C, 75°C, and 85°C respectively during charging while maintained at 25°C during discharging processes. A structured mesh discretizes the computational domain, and a second-order upwind scheme is used for momentum, energy, and turbulence equations. Pressure-velocity coupling is handled by a semi-implicit method. Convergence is checked at each time step, with residuals set to 10^{-4} for continuity, 10^{-5} for velocity components, and 10^{-7} for energy. Multiple mesh sizes (85,000 to 321,000 elements) are tested, with 226,000 elements selected for a balance between accuracy and efficiency as explained in **Fig. 2b**. A time step independent analysis shows minimal differences below 0.2 s, leading to the selection of a 0.1 s time step for accurate results and computational efficiency as demonstrated in **Fig. 2c**.

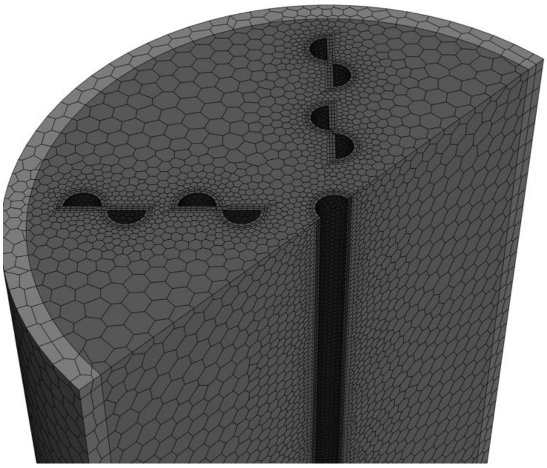

a) Adopted mesh for cases

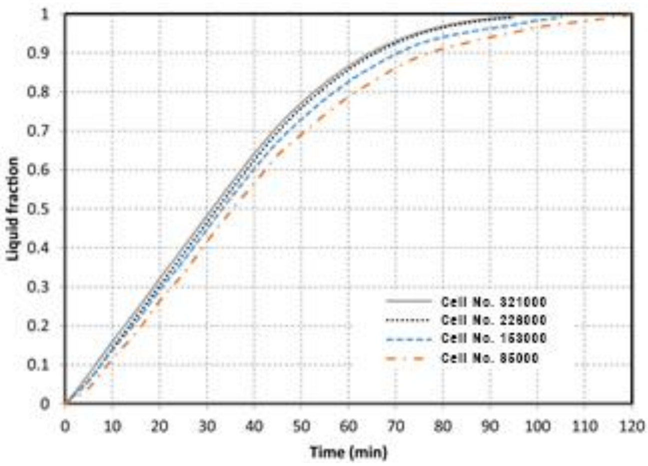

b) Mesh independence test results

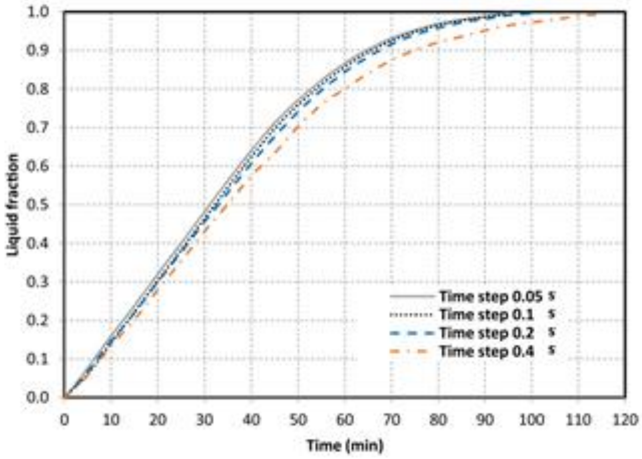

c) Time step independent test results

Fig. 2: Mesh and time step independence analysis adopted for CFD simulations for all cases.

5. NUMERICAL MODEL VALIDATION

The numerical model in this study is validated by comparing its predictions with experimental data conducted on LHTESS [45]. The key validation metric is charging effectiveness (ε_{ch}), using a shell-and-tube heat exchanger with organic paraffin PCM (RT60). This heat exchanger has a cylindrical galvanized steel shell and five copper tubes, one central and four in the outer shell region. The model closely matches experimental data on liquid fraction, with a maximum deviation of 8% at 120 minutes, reducing to 2.8% at 260 minutes, showing strong model reliability. The initial error, attributed to unaccounted losses and parameters in the experimental setup, decreased over time as both systems approached steady-state conditions.

Table 3: Properties of PCM and working conditions adopted in numerical model validation study [45].

Specifications		Value
PCM	Type	RT60
	Latent heat (kJ/kg)	168
	Average melting temperature (°C)	58
HTF	Type	Water
	Inlet temperature (°C)	65
	Reynolds number	964.2
Number of internal tubes		5
Orientation of heat exchanger		Vertical

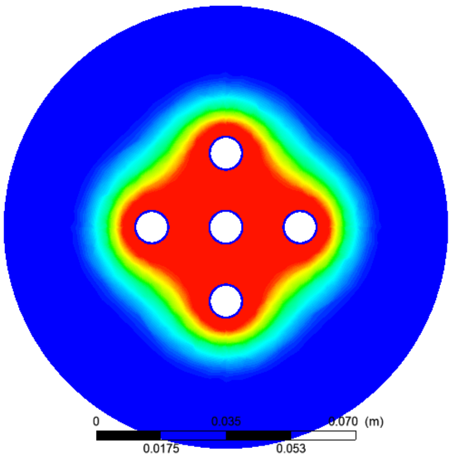

a) Cross section of adopted case.

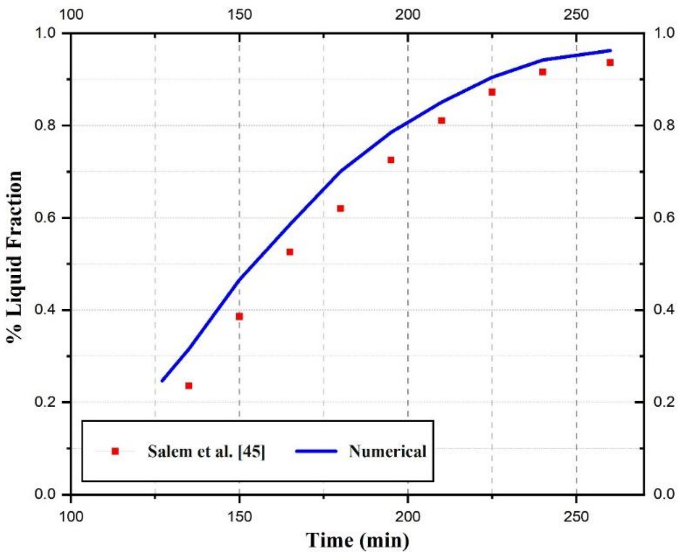

b) Results of validation process.

Fig. 3: Description and results of validiation process for numerical model.

6. HTESS PERFORMANCE

6.1 Impact of Heat Transfer Fluid (HTF) Temperature

This section investigates the effect of varying HTF temperatures (65 °C, 75 °C and 85 °C) on the thermal performance of the LHTESS. A detailed comparison is made focusing on Case 2C, and the charging process performance which is evaluated by the achieved total Melted Mass Fraction (MMS) in each HTF temperature with relative to fixed time, 79 minutes which represented the highest performance and lowest time recorded in this study to achieved 90% MMF, recorded for case 2C with HTF of 85 °C.

As shown in **Fig. 4**, the HTF temperature significantly influences system performance. At an HTF temperature of 85°C, the PCM achieves a 90% fully melted layer, while at 65°C and 75°C, only 28% and 53% MMF recorded, leaving a substantial portion in a solid state. The HTF temperature also affects the temperature distribution within the system. Higher HTF temperatures produce more uniform radial and vertical temperature contours, resulting in a consistent melting pattern throughout the PCM. Additionally, increasing the HTF temperature reduces charging time needed to achieve 90% MMF as following 197 minutes and 109 minutes recording for HTF with temperature 65°C, 75°C and 85°C respectively. Systems operating at 85°C show a reduction in charging time by 55% to 62% compared to those at 65°C. These results underscore the pivotal role of optimizing HTF temperature to enhance charging effectiveness and overall system performance.

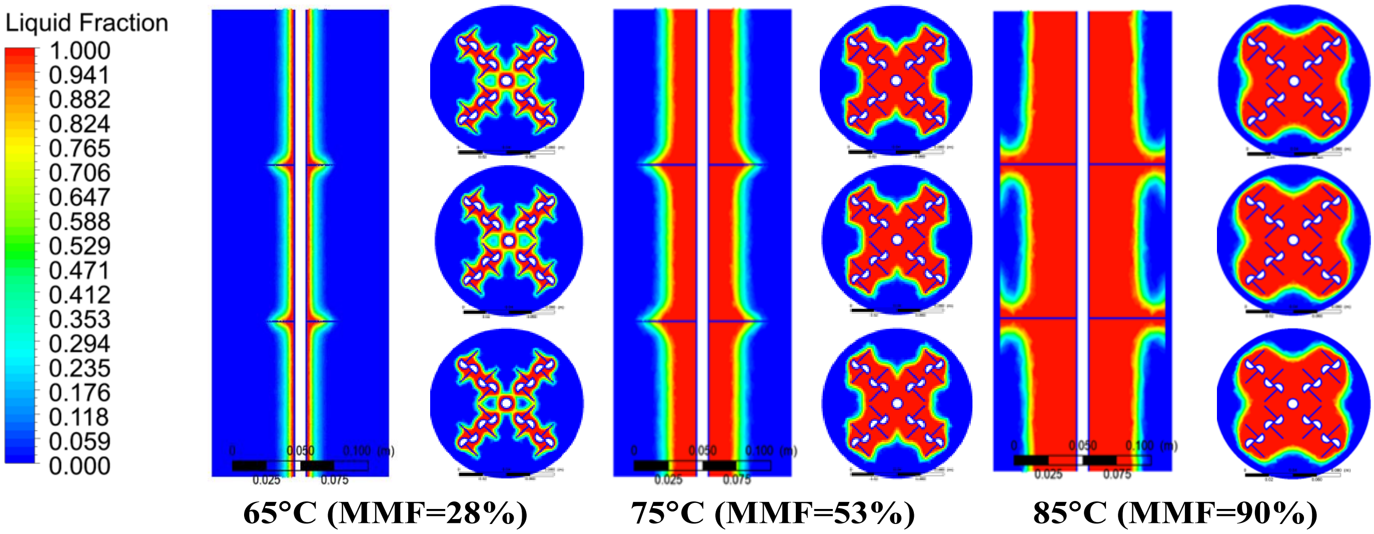

Fig. 4: Influence of HTF inlet temperature on melting fraction contours for Case 2C at reference time 79 minutes of charging time.

6.2 Effect of Conducting Fins

This section provides a detailed comparison of the LHTESS's performance during the charging process, with and without conducting fins on the outer surface of the internal tubes. The analysis is based on a fixed HTF inlet temperature of 75°C and a charging duration of 158 minutes which represented the time required to achieve 90% MMF in Case 2A.

Case 1A represents the baseline configuration without fins, while Case 2A, as shown in **Fig. 1**, includes rectangular straight fins designed to improve thermal performance. The incorporation of fins yields significant improvement by increasing the heat transfer surface area, which leads to a more uniform and effective distribution of thermal energy within PCM. As illustrated in **Fig. 5**, the system equipped with fins (Cases 2A) demonstrates a considerably higher melting fraction compared to the non-finned system (Case 1A). This increased melting fraction highlights the enhanced heat transfer capability of the fined configuration, allowing for more rapid and uniform melting of the PCM.

The fins play a crucial role in optimizing thermal management by facilitating better conduction between the heat transfer fluid and the PCM. This enhanced conduction accelerates PCM's transition from solid to liquid, resulting in a marked improvement in charging effectiveness. The finned system (Case 2A) reduces the charging time to 158 minutes, compared to 224 minutes in the non-finned system (Case 1A) with 75°C HTF, representing an approximately 29.5% reduction in charging duration. This significant reduction in charging time not only demonstrates the fins' effectiveness in enhancing heat transfer but also underscores their ability to improve the overall energy effectiveness of the LHTESS. By optimizing the thermal energy transfer process, the fins contribute to faster PCM melting, improved thermal uniformity, and ultimately, more efficient system performance. This analysis highlights the critical role of fins in reducing thermal resistance and enhancing the operational performance of phase change thermal storage systems.

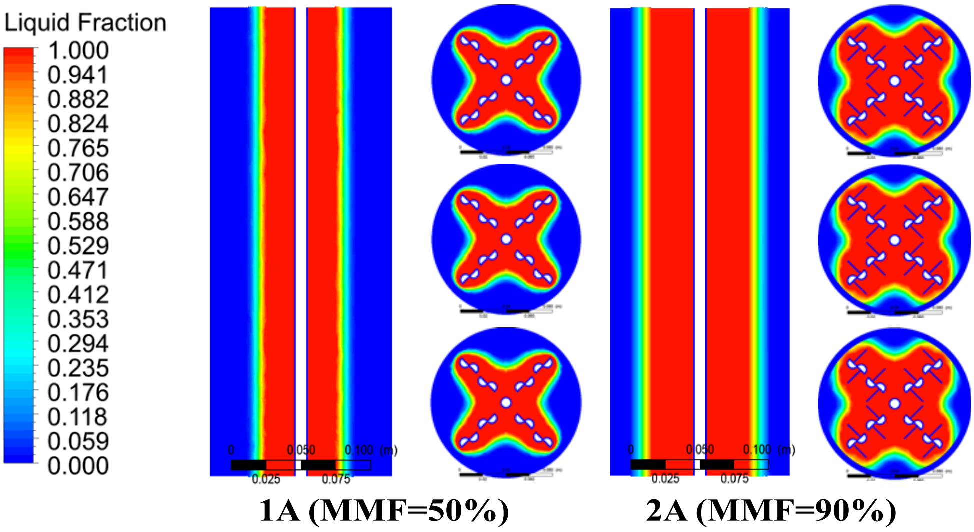

Fig. 5: Comparison of melting fraction contours for finned and non-finned configurations at fixed HTF inlet temperature 75°C and 158 minutes charging time.

6.3 Effect of Conducting Barriers

This section presents key findings for Case 1 during the charging process, with an HTF inlet temperature of 85°C and a charging time of 81 minutes. Case 1A serves as the baseline without barriers, while Cases 1B through 1G incorporate various barrier designs, as depicted in **Fig. 1**. The introduction of barriers significantly enhances the melting fraction of the PCM, as shown in **Fig. 6**. The barriers improve heat transfer by enabling more efficient movement of thermal energy both upward and downward. This results in a more uniform temperature profile across the PCM, accelerating the melting process and improving overall thermal performance. Comparing full-barrier and half-barrier configurations reveals that barrier length plays a crucial role in optimizing thermal effectiveness. Full-barrier cases show a higher melting fraction and shorter charging times, with a maximum difference of 64 minutes between the longest (Case 1A) and shortest (Case 1C) charging times, reflecting an approximate time reduction of 80%. Full barriers create optimal conditions for heat transfer, speeding up the phase change process within the PCM. Among the full-barrier designs, Case 1C, which divides the shell into equal volumes, is the most effective case. This configuration ensures an even distribution of thermal energy throughout PCM, resulting in faster and more consistent melting. In contrast, designs like Case 1E and 1G which do not divide the shell into equal volumes, lead to less efficient heat transfer due to uneven volume distribution, causing thermal imbalances and slower melting rates in certain regions.

Case 1C, with its balanced heat transfer pathways, allows for faster and more uniform melting, significantly reducing charging time and increasing the melting fraction per unit volume of the shell. The improved effectiveness of this design highlights the importance of optimizing barrier design. Additionally, parallel-barrier designs (Cases 1B, 1C, and 1E) outperform non-parallel configurations, providing more uniform heat transfer across the PCM. However, Case 1C, which divides the shell into equal volumes, outperforms other parallel designs, offering an optimal balance between heat distribution and melting rate.

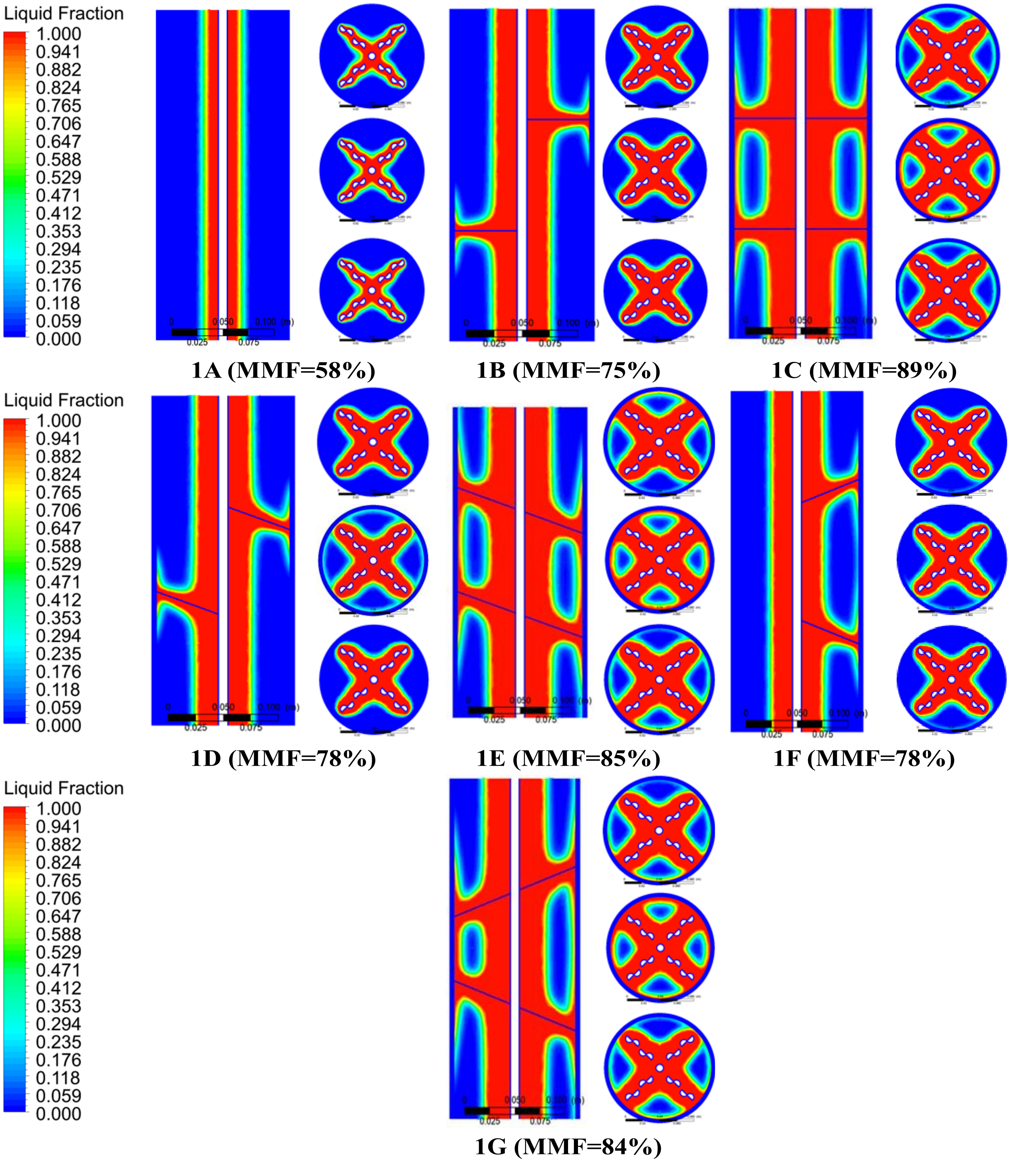

Fig. 6: Melting fraction contours for diverse barrier configurations in Case 1 (without fins) at fixed HTF inlet temperature 85°C over 81 minutes of charging progress.

6.4 Combined Influence of Barriers and Fins

This section offers a comprehensive analysis of LHTESS's performance, focusing on results obtained with an HTF inlet temperature of 75°C as a representative sample. The system integrates fins on the outer surface of internal tubes with barriers in the shell-side, compared to the base case (1A) that lacks both fins and barriers, and cases (1B to 1G), which include only barriers. The analysis covers a charging period of 109 minutes, with **Fig. 7** shows the comparison between Cases

1A, 1C, and 2C. This sample highlights how the combination of fins and barriers dramatically improves the PCM melting process. Fins increase the heat transfer surface area, facilitating better conduction into the PCM, while barriers promote effective heat distribution by guiding thermal energy throughout the shell, eliminating stagnant zones and improving thermal uniformity. The joint effect of these enhancements leads to faster melting and a higher melting fraction over a shorter period.

Case 2C demonstrates superior performance, achieving a 90% liquid fraction within 109 minutes, whereas the base case takes 203 minutes to reach the same melting fraction. The significant reduction in charging time underscores the effectiveness of the combined conductive enhancement from fins and convective control provided by barriers, which together reduce the charging time by nearly 50%. Additionally, the melting fraction increases by 30% to 46%, depending on the configuration. This result, while presented for one specific temperature, reflects broader trends observed under various operational conditions. The improvements in melting speed and thermal performance evident in this sample case are consistent with results across other scenarios. The combination of fins and barriers significantly enhances the system's thermal performance, demonstrating the robustness of this approach in improving both melting rates and temperature distribution across different operating environments. Case 2C exemplifies the optimal balance between conductive and convective heat transfer, allowing for faster phase change and uniform heat distribution. These results underscore the value of integrating fins and barriers to achieve superior thermal management, optimizing both charging time and melting fraction for more efficient latent heat thermal energy storage.

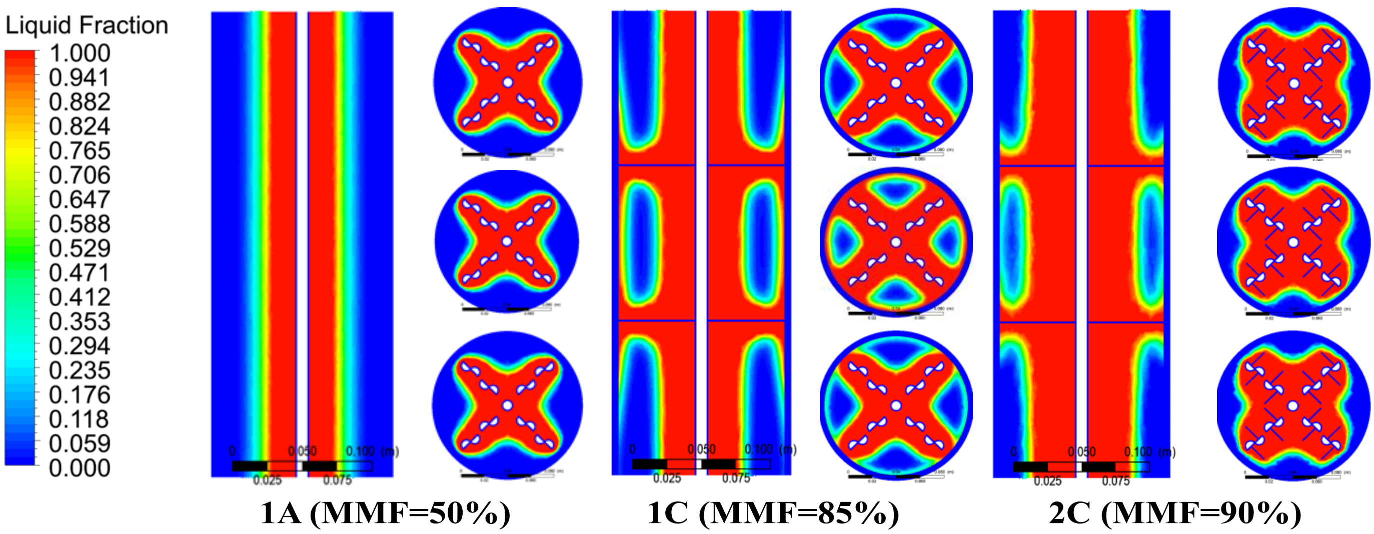

Fig. 7: Barriers and their combination at HTF inlet temperature 75°C and 109 min charging time.

Fig. 8 illustrates the charging times for various study cases conducted at HTF inlet temperature of 85°C. Case 2C exhibits the most efficient performance, achieving a 90% liquid fraction for the PCM in just 79 minutes. Closely following are Cases 2E and 2G, both reaching the same liquid fraction in 81 minutes. The other cases, ordered by charging time, are 1C (89 minutes), 1E (91 minutes), 1G (99 minutes), 2D (99 minutes), 2B (100 minutes), 2F (110 minutes), 2A (117 minutes), 1F (117 minutes), 1D (117 minutes), 1B (145 minutes), and finally 1A (145 minutes). Notably, the difference in charging time between the shortest case (2C) and the longest case (1A) is a significant 66 minutes.

The time reduction ratio, calculated as the difference in charging time between each case and the longest case (1A), reflects charging process performance. **Fig. 9** presents these results for the HTF inlet temperature of 85°C. The analysis reveals that Case 1F has the minimum performance at 19.3%, while Case 2C boasts the highest performance at 45.5%. This underscores the importance of optimizing charging conditions to enhance the performance of LHTESSs. It is noteworthy that Case 1A consistently stands for the least efficient configuration, whereas Case 2C shows the best charging performance. The reduction in charging time has a significant impact on the inlet water temperature. For example, the charging time for the least efficient case, 1A, decreases from 409 minutes at an inlet water temperature of 65°C to just 145 minutes at 85°C, reflecting a remarkable reduction of 264 minutes and an effectiveness increase of 64.54%. Similarly, the best-performing case, 2C, gives charging time drop from 197 minutes at 65°C to 79 minutes at 85°C, resulting in a difference of 118 minutes and an effectiveness improvement of 59.60%. This highlights the substantial impact that higher inlet water temperatures have on the thermal performance of these systems.

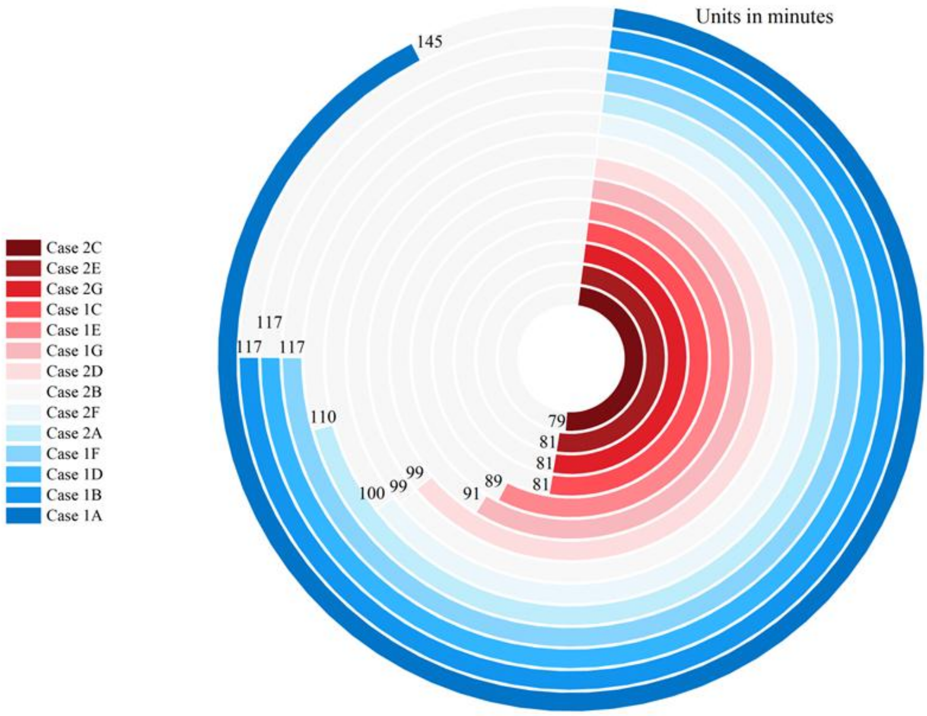

Fig. 8: Comparison of charging times for different configurations at HTF inlet temperature 85°C.

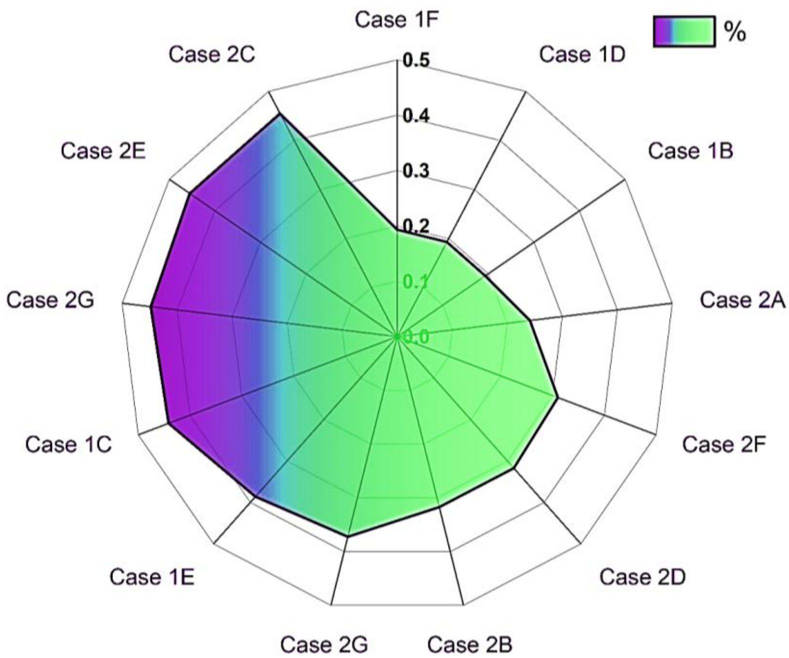

Fig. 9: Charging time reduction ratio at HTF inlet temperature 85°C.

CONCLUSIONS

This study numerically investigates the performance of an LHTESS by analyzing various configurations and operational parameters. The findings offer critical insights into refining thermal performance and reducing charging times through adjustments in HTF temperatures, the incorporation of conducting fins, and the implementation of conducting barriers. Higher HTF temperatures significantly improve thermal performance. For instance, at an HTF inlet temperature of 85°C, a 90% melting fraction is achieved within 79 minutes, compared to only a 28% melting fraction at 65°C. This improvement is attributed to the more uniform radial and vertical temperature contours at higher HTF temperatures, resulting in consistent melting patterns across the PCM. The integration of conducting fins further enhances the system's performance by reducing charging times. Specifically, charging time decreases by 31% at an HTF inlet temperature of 65°C, by 29.5% at 75°C, and by 24.5% at 85°C. This improvement is due to the increased heat transfer surface area provided by the fins, which enhances thermal conductivity and accelerates the melting process. Conducting barriers also play a pivotal role in improving the melting fraction and charging time. Full-barrier configurations significantly outperform half-barrier designs, with melting fractions of 37.21%, 38.62%, and 44.13% observed in cases G, E, and C, respectively, compared to 19.31% for half-barrier designs at an HTF temperature of 85°C. Full parallel barriers demonstrated the best performance due to their ability to increase the heat transfer surface area and improve heat distribution, resulting in shorter charging times and higher efficiency. The combined integration of fins and barriers yields the most substantial performance enhancements. Case 2C exhibited the highest effectiveness, achieving melting fractions of 45.5%, 46.82%, and 51.5% for HTF inlet temperatures of 85°C, 75°C, and 65°C, respectively. These results underscore the synergistic effects of fins and barriers, which increase the total heat transfer surface area and improve thermal performance. Improving HTF temperatures and strategically incorporating fins and barriers significantly enhance the overall performance of LHTESS, aligning with the study's goals and offering valuable insights into future applications and designs. For future work, experimental validation of Case 2C is recommended to confirm the numerical findings. Additionally, investigating the influence of incorporating nanomaterials into PCM for Case 2C could provide further opportunities for performance enhancement.

REFERENCES

[1] M. Khodadadi, M. Sheikholeslami, “Efficiency and electrical performance evaluation of photovoltaic unit under influence of NEPCM”, International Journal of Heat Mass Transfer, Vol. 183, Article 122232, 2022.

[2] S. Algarni, T. Alqahtani, K. Almutairi, “Experimental investigation of an evacuated tube solar collector incorporating nano-enhanced PCM as a thermal booster”, Applied Thermal Energy, Vol. 180, Article 115831, 2020.

[3] T. Long, W. Li, Y. Lv, Y. Li, S. Liu, J. Lu, S. Huang, Y. Zhang, “Benefits of integrating phase-change material with solar chimney and earth-to-air heat exchanger system for passive ventilation and cooling in summer”, Journal of Energy Storage, Vol.48, Article 104037, 2022.

[4] M.R. Salem, M.M. Elsayed, A.A. Abd-Elaziz, K.M. Elshazly, “Performance enhancement of the photovoltaic cells using Al2O3/PCM mixture and/or water cooling-techniques”, Renewable Energy, Vol. 138, pp. 876-890, 2019.

[5] S. Cesari, G. Emmi, M. Bottarelli, “A weather forecast-based control for the improvement of PCM enhanced radiant floors”, Applied Thermal Engineering, Vol. 206, Article 118119, 2022.

[6] A.O. Eldokaishi, M.Y. Abdelsalam, M.M. Kamal, H.A. Abotaleb, “Modeling of water PCM solar thermal storage system for domestic hot water application using Artificial neural networks”, Applied Thermal Engineering, Vol. 204, Article 118009, 2022.

[7] S. Rostami, M. Afrand, A. Shahsavar, M. Sheikholeslami, “A review of melting and freezing processes of PCM / nano-PCM and their application in energy storage”, Energy, El Sevier Energy, Vol. 211, Article 118698, 2020

[8] C. Nie, J. Liu, S. Deng, “Effect of geometry modification on the thermal response of composite metal foam phase change material for thermal energy storage”, International Journal of Heat and Mass Transfer, Vol. 165, Article 120652, 2021.

[9] K. Kahveci, U. Akyol, E. Akyol, “Experimental and numerical investigation of heat transfer in a channel with multiple phase change materials (PCMs)”, Journal of Energy Storage, Vol. 45, Article 103710, 2022.

[10] A. Kumar, P. Verma, L. Varshney, “An experimental and numerical study on phase change material melting rate enhancement for a horizontal semicircular shell and tube thermal energy storage system”, Journal of Energy Storage, Vol. 45, Article 103734, 2022.

[11] A. Shahsavar, A.H. Majidzadeh, R.B. Mahani, P. Talebizadehsardari, “Entropy and Thermal performance Analysis of PCM Melting and Solidification Mechanisms in a Wavy Channel Triplex-Tube Heat Exchanger”, Elsevier Renewable Energy, Vol. 165-2, P 52-72, 2021.

[12] M. Asker, H. Ganjehsarabi, C.M. Turhan, “Numerical investigation of inward solidification inside spherical capsule by using temperature transforming method”, Ain Shams Engineering Journal, Vol. 9, pp. 537 – 547, 2018.

[13] R. Zhu, D. Jing, “Numerical study on thermal and melting performances of a horizontal latent heat storage unit with branched tree-like convergent fins”, Energy Storage, Vol. 62, Article 106889, 2023.

[14] M. Asker, E. Alptekin, M.A. Ezan, H. Ganjehsarabi, “Entropy generation analysis of multilayer PCM slabs integrated with fins”, Int. J. Exergy, Vol. 26, pp.154-169, 2018.

[15] P. Sardari, H. Mohammed, D. Giddings, G. Walker, M. Gillott, D. Grant, Numerical study of a multiple-segment metal foam-PCM latent heat storage unit: Effect of porosity, pore density and location of heat source, Energy, Vol. 189, Article 116108, 2019.

[16] M.A. Essa, I.Y. Rofaiel, M.A. Ahmed, “Experimental and Theoretical Analysis for the Performance of Evacuated Tube Collector Integrated with Helical Finned Heat Pipes using PCM Energy Storage”, El Sevier Energy, Vol. 206, Article 118166, 2020.

[17] B. Peng, Z. He, H. Wang, F. Su, “Optimization of patterned-fins for enhancing charging performances of phase change materials-based thermal energy storage systems”, International Journal of Heat and Mass Transfer, Vol.164, Article 120573, 2021.

[18] R. Qaiser, M. Mahabat, L. Asip, M. Irfan, “Melting performance enhancement of PCM based thermal energy storage system using multiple tubes and modified shell designs”, El Sevier Energy Storage, Vol. 33, Article 102161, 2021.

[19] R. Elarem, T. Alqahtani, S. Mellouli, W. Aich, “Numerical study of an Evacuated Tube Solar Collector incorporating a Nano-PCM as a latent heat storage system”, Case Studies in Thermal Engineering, Vol. 24, Article 100859, 2021.

[20] J. Ma, H. Xu, S. Liu, H. Peng, X. Ling, “Numerical study on solidification behavior and exergy analysis of a latent heat storage unit with innovative circular superimposed longitudinal fins”, International Journal of Heat and Mass Transfer, Vol. 169, Article 120949, 2021.

[21] G.S. Sodhi, P. Muthukumar, “Compound charging and discharging enhancement in multi-PCM system using non-uniform fi n distribution”, Renewable Energy, Vol. 171, pp. 299-314, 2021.

[22] K. Kant, P.H. Biwole, A. Shukla, A. Sharma, S. Gorjian,“Heat transfer and energy storage performances of phase change materials encapsulated in honeycomb cells”, Journal of Energy Storage, Vol. 38, Article 102507, 2021.

[23] I. Sarani, S. Payan, S.A. Nada, A. Payan, “Numerical investigation of an innovative discontinuous distribution of fins for solidification rate enhancement in PCM with and without nanoparticles”, Applied Thermal Engineering, Vol.176, Article 115017, 2020.

[24] L. A. Khan, K. M. Mahabat, “Role of orientation of fins in performance enhancement of a latent thermal energy storage unit”, Applied Thermal Energy, Vol.175, Article 115408, 2020.

[25] M.R. Hajizadeh, A.N. Keshteli, Q. Bach, “Solidification of PCM within a tank with longitudinal-Y shape fins and CuO nanoparticle”, Journal of Molecular Liquids, Vol. 317, Article 114188, 2020.

[26] J. Duan, Y. Xiong, D. Yang, “Study on the effect of multiple spiral fins for improved phase change process”, Applied Thermal Engineering. Eng., Vol.169, Article 114966, 2020.

[27] D.S. Mehta, B. Vaghela, M.K. Rathod, J. Banerjee, “Thermal performance augmentation in latent heat storage unit using spiral fin: An experimental analysis”, Journal of Energy Storage, Vol.31, Article 101776, 2020.

[28] M. Carmona, A. Palacio, J.E. Doria, “Experimental evaluation of a hybrid photovoltaic and thermal solar energy collector with integrated phase change material (PVT-PCM) in comparison with a traditional photovoltaic (PV) module”, Renewable Energy, Vol. 172, pp. 680-696, 2021.

[29] S. Yao, X. Huang, “Study on solidification performance of PCM by longitudinal triangular fins in a triplex-tube thermal energy storage system”, El Sevier Energy, Vol. 227, Article 120527, 2021.

[30] X. Huang, S. Yao, “Solidification performance of new trapezoidal longitudinal fins in latent heat thermal energy storage". Case Studies, Therm. Eng., Vol.26, Article 101110, 2021.

[31] Y. Huang, X. Liu, “Charging and discharging enhancement of a vertical latent heat storage unit by fractal tree-shaped fins”, Renewable Energy, Vol. 174, pp. 199–217, 2021.

[32] F. Hasnain, M. Irfan, K.M. Mahabat, K.L. Asip, A.H. Farooq, “Melting performance enhancement of a phase change material using branched fins and nanoparticles for energy storage applications”, Journal of Energy Storage, Vol. 38, Article 102513, 2021.

[33] L.A. Khan, M.M. Khan, H. Ahmed, F. Irfan, D. Brabazon, “Dominant roles of eccentricity, fin design, and nanoparticles in performance enhancement of latent thermal energy storage unit”, Journal of Energy Storage, Vol.43, Article 103181, 2021.

[34] A.M. Abdulateef, M. Jaszczur, Q. Hassan, R. Anish, H. Niyas, K. Sopian, et al., “Enhancing the melting of phase change material using a fin–nanoparticle combination in a triplex tube heat exchanger”, Journal of Energy Storage, Vol.35, Article 102227, 2021.

[35] B. Lu, Y. Zhang, D. Sun, Z. Yuan, S. Yang, “Experimental investigation on thermal behavior of paraffin in a vertical shell and spiral fin tube latent heat thermal energy storage unit”, Applied Thermal Engineering, Vol.187, Article 116575, 2021.

[36] D.S. Mehta, B. Vaghela, M.K. Rathod, J. Banerjee, “Heat transfer enhancement using spiral fins in different orientations of Latent Heat Storage Unit”, International Journal of Thermal Sciences, Vol.169, Article 107060, 2021.

[37] J. Guo, Z. Liu, B. Yang, X. Yang, J. Yan, “Melting assessment on the angled fin design for a novel latent heat thermal energy storage tube”, Renewable Energy, Vol.183, pp. 406-422, 2022.

[38] X. Luo, J. Gu, H. Ma, Y. Xie, A. Li, J. Wang, R. Ding, “Numerical study on enhanced melting heat transfer of PCM by the combined fractal fins”, Journal of Energy Storage, Vol.45, Article 103780, 2022.

[39] X. Tianhao, N. H. Emma, T. Silvia, I. Monika, S. Samer, C. Justin “Experimental and numerical investigation of a latent heat thermal energy storage unit with ellipsoidal macro-encapsulation”, Energy, Vol. 238, Article 121828, 2022.

[40] M. Tiji, W. Al-Azzawi, H. Mohammed, A. Dulaimi, F. Rashid, J. Mahdi, H. Majdi, P. Talebizadehsardari, H. Ali, Thermal management of the melting process in a latent heat triplex tube storage system using different configurations of frustum tubes, Journal of Nanomaterials, Vol. 2022(1), Article 7398110, 2022.

[41] A. Abed, H. Mouziraji, J. Bakhshi, A. Dulaimi, H. Mohammed, R. Ibrahem, N. Khedher, W. Yaïci, J. Mahdi, Numerical analysis of the energy-storage performance of a PCM-based triplex-tube containment system equipped with arc-shaped fins, Front Chem., Vol. 10, Article 1057196, 2022.

[42] N. Khedher, H. Togun, A. Abed, H. Al-Najjar, A. Dulaimi, H. Mohammed, J. Mahdi, A. Yvaz, P. Talebizadehsardari, Discharge performance assessment of a vertical double-pipe latent heat storage unit equipped with circular Y-shaped fins, Journal of Building Engineering, Vol. 75, Article 106870, 2023.

[43] H. Xu, H. Zuo, K. Zeng,Y. Lu, J. Kong, B. Chi, J. Gao, H. Yang, H. Chen “The heat transfer enhancement of the converging-diverging tube in the latent heat thermal energy storage unit: Melting performance and evaluation”, Energy, Vol. 282, Article 128937, 2023.

[44] B. Nicola, C. Martina, F. Andrea, I. Marcello, M.M. Gerardo, M. Luigi “Thermal analysis of micro-encapsulated phase change material (MEPCM)-based units integrated into a commercial water tank for cold thermal energy storage”, Energy, Vol. 266, Article 126479,2023.

[45] M.R. Salem, M.N. Owyed, R.K. Ali, “Experimental investigation of the performance attributes of a thermal energy storage unit using different system configurations”, Applied Thermal Engineering, Vol. 230, Article 120678, 2023.

[46] O. Younis, M. Mozaffari, A. Ahmed, M. Ghalambaz, M. Ghalambaz, Improvement of latent heat thermal energy storage rate for domestic solar water heater systems using anisotropic layers of metal foam, Buildings, 14(8), 2322, 2024.

[47] L. Jialing, R. Zuhair, N. Mohammed, S. Kamal, N. Hakeem, M. Hazim, A. Akbar, “Effect of twisted fins on the melting performance of PCM in a latent heat thermal energy storage system in vertical and horizontal orientations: Energy and exergy analysis”, Applied Thermal Engineering, Vol. 219, Article 119489, 2023.

[48] M.S. Mahdi, A.F. Hasan, H.B. Mahood, A.N. Campbell, A. A. Khadom, A. M. Karim, et al., “Numerical study and experimental validation of the effects of orientation and configuration on melting in a latent heat thermal storage unit”, Journal of Energy Storage, Vol. 23, pp. 456-468, 2019.

[49] N. Kousha, M.J. Hosseini, M.R. Aligoodarz, R. Pakrouh, R. Bahrampoury, “Effect of inclination angle on the performance of a shell and tube heat storage unit – An experimental study”, Applied Thermal Engineering, Vol. 112, pp. 1497-1509, 2017.